frontiers | Frontiers in Earth Science

TYPE Original Research
PUBLISHED 07 October 2022
DOI 10.3389/feart.2022.994580

OPEN ACCESS

EDITED BY
Nobuaki Fuji,
UMR7154 Institut de Physique du Globe de Paris (IPGP), France

REVIEWED BY
Tushar Mittal,
Massachusetts Institute of Technology, United States
Karoly Nemeth,
Massey University, New Zealand

*CORRESPONDENCE
Kenta Ueki,
kenta_ueki@jamstec.go.jp

SPECIALTY SECTION
This article was submitted to Geochemistry, a section of the journal Frontiers in Earth Science

RECEIVED 15 July 2022
ACCEPTED 14 September 2022
PUBLISHED 07 October 2022

CITATION
Ueki K, Hino H and Kuwatani T (2022), Extracting the geochemical characteristics of magmas in different global tectono-magmatic settings using sparse modeling.
Front. Earth Sci. 10:994580.
doi: 10.3389/feart.2022.994580

Extracting the geochemical characteristics of magmas in different global tectono-magmatic settings using sparse modeling

Kenta Ueki[1]*, Hideitsu Hino[2] and Tatsu Kuwatani[1]

[1]Research Institute for Marine Geodynamics, Japan Agency for Marine-Earth Science and Technology, Yokosuka, Kanagawa, Japan, [2]The Institute of Statistical Mathematics, Tachikawa, Tokyo, Japan

In this study, key geochemical features of magmas formed in eight different tectono-magmatic settings (mid-ocean ridges, oceanic islands, oceanic plateaus, continental flood basalt provinces, intra-oceanic arcs, continental arcs, island arcs, and back-arc basins) are presented that were obtained using a machine-learning-based statistical model. We analyzed geochemical data for volcanic rocks compiled from the global geochemical databases based on statistical model fitting. We used the sparse modeling approach, with which we can objectively identify a small number of fundamental features from a large number of observations. This approach allowed us to identify a small number of representative geochemical features from a total of 857 variables, including major and trace element concentrations, isotope ratios, and all possible ratios and multiplications of elements. Based on the statistical analysis, we present a small number (2–4) of key geochemical features for each tectono-magmatic setting. The extracted geochemical features and associated diagrams can be used to examine geochemical similarities and differences between tectono-magmatic settings and to identify the geochemical characteristics of unknown samples. Based on the extracted geochemical characteristics, we discuss the processes that may lead to the formation of magmas in different tectono-magmatic settings. Our statistical analysis shows that the geochemical signatures of magmas vary with the tectono-magmatic setting, as do the geochemical processes involved in magma generation.

KEYWORDS

tectono-magmatic settings, machine learning, geochemical features of magmas, magma generation processes, feature extraction

1 Introduction

Present-day terrestrial magmatism is closely linked to plate tectonics and mantle dynamics (Wilson, 2007). Understanding the geochemical characteristics of magmas generated in different tectono-magmatic settings is key to understanding how plate tectonics and mantle dynamics have driven magma generation and the geochemical

evolution of Earth (e.g., Wyllie, 1988; Stracke, 2012). The geochemistry of volcanic rocks, including the concentrations and ratios of major and trace elements, and isotopic data, provides insights into the key processes involved in magma generation, such as melting conditions, source components, and the involvement of and mixing between specific mantle and crustal components (Plank and Langmuir, 1988; Hofmann, 1997; Pearce et al., 2005). To identify and compare the geochemical processes involved in magma generation in different tectono-magmatic settings, it is important to determine a small number of key geochemical proxies from the full spectrum of available geochemical data. However, if major and trace elements and their ratios, multiplications, and isotope ratios were all considered, then this would result in at least several hundred variables.

Recently, statistical approaches based on machine learning (ML) have been used to solve various geochemical problems (e.g., Petrelli and Perugini, 2016; Ueki et al., 2018; Zhao et al., 2019; Itano et al., 2020). One objective of the ML approach is to analyze large multi-dimensional data sets with high precision, and we previously conducted this type of analysis in order to discriminate between magmas formed in different tectono-magmatic settings (Ueki et al., 2018). A further objective of the ML approach is "feature extraction", which objectively selects a small number of key features from the input data. In this study, we conducted a ML-based feature extraction to explore and interpret geochemical data based on multi-dimensional data, including major and trace elements, combinations of elements (i.e., elemental ratios and multiplications), and isotope ratios.

In this study, we present a statistical methodology applicable to geochemistry, which is a "smart model selection" technique. A popular statistical model based on the sparse modeling approach (Tibshirani, 1996), which is called sparse multinomial logistic regression (SMR), is used to extract a small number of key geochemical features from volcanic rocks generated in different tectono-magmatic settings. We considered eight tectonic settings (mid-ocean ridges, oceanic islands, oceanic plateaus, continental flood basalt provinces, continental arcs, island arcs, intra-oceanic arcs, and back-arc basins) and a total of 857 geochemical variables, including the concentrations, ratios, and multiplications of major and trace elements, and isotope ratios. We show that our statistical method can objectively identify a small number of key geochemical variables from high-dimensional geochemical datasets. Based on these, we discuss the geochemical processes associated with magma generation processes in different tectono-magmatic settings. Due to the sparsity and linearity of the statistical approach, the geochemical significance of each key feature can be readily interpreted, and thus the model enables us to obtain insights into magma generation from geochemical data.

2 Methods

This study involved feature extraction from different classes (i.e., tectono-magmatic settings). We used geochemical datasets for volcanic rocks collected from well-characterized tectonic settings. Following Li et al. (2015), we considered eight tectono-magmatic settings: mid-ocean ridges (MOR), oceanic islands (OI), oceanic plateaus (OP), continental flood basalts (CFB), continental arcs (CA), island arcs (IA), intra-oceanic arcs (IOA), and back-arc basins (BAB). Twenty-nine elements and isotope ratios were considered: 8 major elements (SiO_2, TiO_2, Al_2O_3, Fe_2O_3, CaO, MgO, Na_2O, and K_2O; in wt%), along with 16 selected trace elements (Sr, Ba, Rb, Zr, Nb, La, Ce, Nd, Hf, Sm, Gd, Y, Yb, Lu, Ta, and Th; in ppm) and five isotope ratios ($^{206}Pb/^{204}Pb$, $^{207}Pb/^{204}Pb$, $^{208}Pb/^{204}Pb$, $^{87}Sr/^{86}Sr$, and $^{143}Nd/^{144}Nd$).

Our dataset is based on our previous study (Ueki et al., 2018), which included volcanic-rock geochemical data compiled from the global geochemical databases PetDB (http://www.earthchem.org/petdb) and GEOROC (http://georoc.mpch-mainz.gwdg.de/georoc/). Ueki et al. (2018) compiled volcanic rock samples with complete data for the above mentioned 8 major, 16 trace and five isotopic data. Data published after 1990 AD were used to minimize analytical uncertainties, and samples marked as altered were excluded from our analysis. Only Quaternary samples were compiled for arc settings. Major elements were normalized to 100% anhydrous compositions with total Fe expressed as Fe_2O_3. Ueki et al. (2018) used the measured isotope ratios as input data for a source discrimination problem for an unknown sample. In the present study, we use the age-corrected initial isotope ratios for the CFB and OP settings. If the initial isotope ratios were not reported, we conducted age corrections using the reported whole-rock Sr, Rb, Nd, Sm, U, Th, and Pb concentrations and ages of the rocks. The half-lives and relative atomic masses of isotopes used for these calculations are from Holden et al. (2018). Age-corrected isotope ratios for OP and CFB samples are listed in Supplementary Table S1. We have removed samples for which these values were not reported in the original dataset (Ueki et al., 2018). Data showing noticeable outliers in the corrected isotope ratios were also excluded. As a result, a total of 2,063 samples were considered in our analysis. The locations of the samples are shown in Figure 1. Bivariate diagrams showing variations in selected major element concentrations and isotope ratios are shown in Figure 2. The dataset is available on GitHub (https://github.com/hideitsu/geoSMR) and the Supplementary Material.

We considered all possible combinations (i.e., ratios and multiplications) of 24 major and trace elements, which results in ${}_{24}C_2$ patterns for multiplications and ${}_{24}P_2$ patterns for ratios. Consequently, the total number of variables is 857

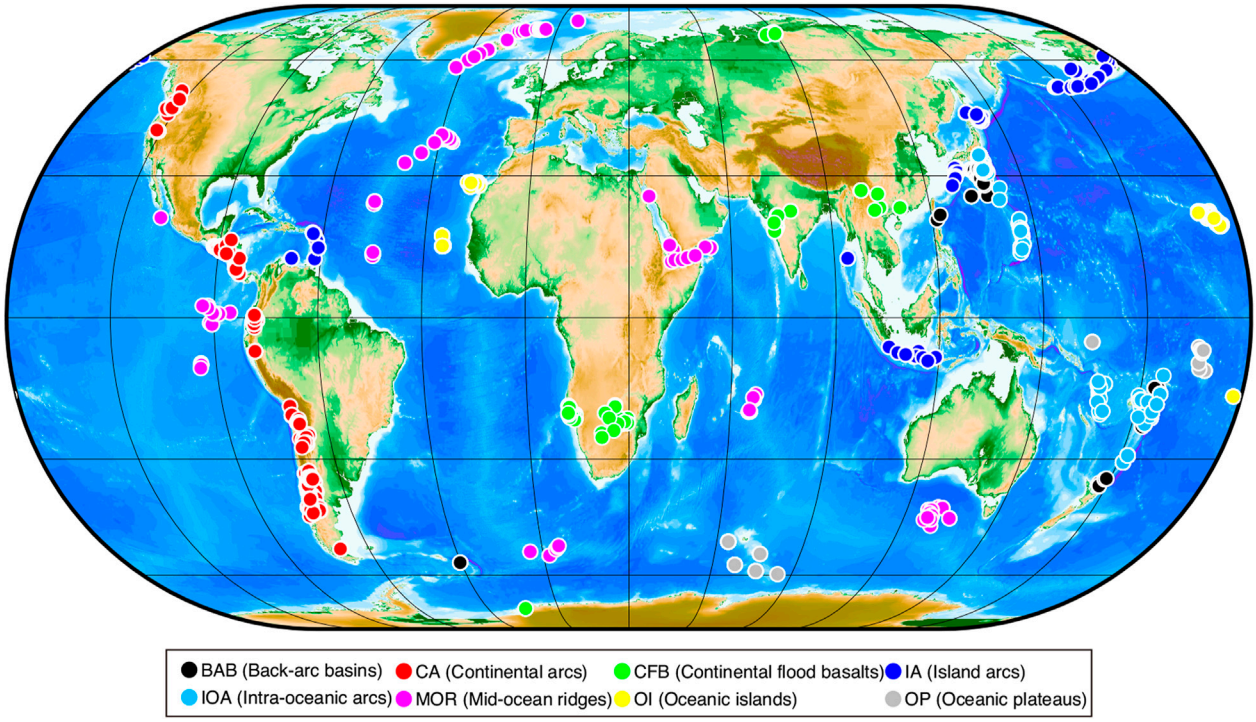

FIGURE 1
Map showing the locations of samples used in this study. Topographic data are from TerrainBase (National Geophysical Data Center/NESDIS/NOAA/U.S. Department of Commerce, 1995).

(= 29 + ${}_{24}C_2$ + ${}_{24}P_2$). We objectively extracted a small number of key geochemical features of each tectono-magmatic setting from these 857 variables. Input data (i.e., elemental concentrations, ratios, and multiplications, and isotope ratios) were normalized using a one-parameter Box–Cox transformation (Box and Cox, 1964) before fitting the statistical model.

Feature extraction in this study is based on selection of the statistical model that best fits the input data. For feature extraction, we used sparse multinomial logistic regression (SMR), which is a sparse variant of the generalized linear model (Nelder and Wedderburn, 1972). SMR allows for the high-dimensional classification of different classes. Furthermore, the use of statistical modeling based on SMR allows us to extract a small number of key geochemical features and discriminate among tectono-magmatic settings (Ueki et al., 2018). This approach uses a set of projection vectors $\boldsymbol{w}^{(k)}$ to classify the sample as follows:

$$\left(\boldsymbol{w}^{(k)}\right)^{\top}\boldsymbol{x} = w_0^{(k)} + w_1^{(k)}x_1 + \cdots + w_p^{(k)}x_p, \quad k = 1, \ldots, C \tag{1}$$

where $\boldsymbol{x}$ denotes the compositional vector that consists of major and trace element concentrations, ratios, and multiplications, and isotope ratios of a sample. Using this vector, the compositional vector $\boldsymbol{x}$ is projected onto the eight sub-spaces (i.e., the tectono-magmatic settings). $\boldsymbol{w}$ (projection vectors) provides information on the variables that are important to characterize the different settings. Given that we consider eight tectonic settings (C = 8) and 857 variables (p = 857), we must consider a maximum $\boldsymbol{w}$ value of 6,864 (= 8 × 857 + 8 constant terms). In multinomial logistic regression, the probability that the input variable $\boldsymbol{x}$ belongs to the kth class is defined as follows:

$$\Pr\left(c\left(\boldsymbol{x}\right) = k\right) = \frac{\exp\left(\boldsymbol{w}^{(k)\top}\boldsymbol{x}\right)}{\sum_{l=1}^{C}\exp\left(\boldsymbol{w}^{(l)\top}\boldsymbol{x}\right)}, \tag{2}$$

where $c(\boldsymbol{x})$ denotes the class of $\boldsymbol{x}$; for the observed samples $\{\boldsymbol{x}_i, c\left(\boldsymbol{x}_i\right)\}_{i=1}^{n}$, its log-likelihood is given by:

$$\begin{aligned} l\left(\boldsymbol{w}\right) &= \log\prod_{i=1}^{n}\frac{\exp\left(\boldsymbol{w}^{(t(i))\top}\boldsymbol{x}\right)}{\sum_{l=1}^{C}\exp\left(\boldsymbol{w}^{(l)\top}\boldsymbol{x}\right)} \\ &= \sum_{i=1}^{n}\left\{\boldsymbol{w}^{(t(i))\top}\boldsymbol{x}_i - \log\left(\sum_{l=1}^{C}\exp\left(\boldsymbol{w}^{(l)\top}\boldsymbol{x}_i\right)\right)\right\}, \end{aligned} \tag{3}$$

where $t(i) = c(\boldsymbol{x}_i)$. Because we are only interested in a small number of elements that characterize the different tectono-magmatic settings, and the number of parameters is larger than the number of observations, we use the sparse

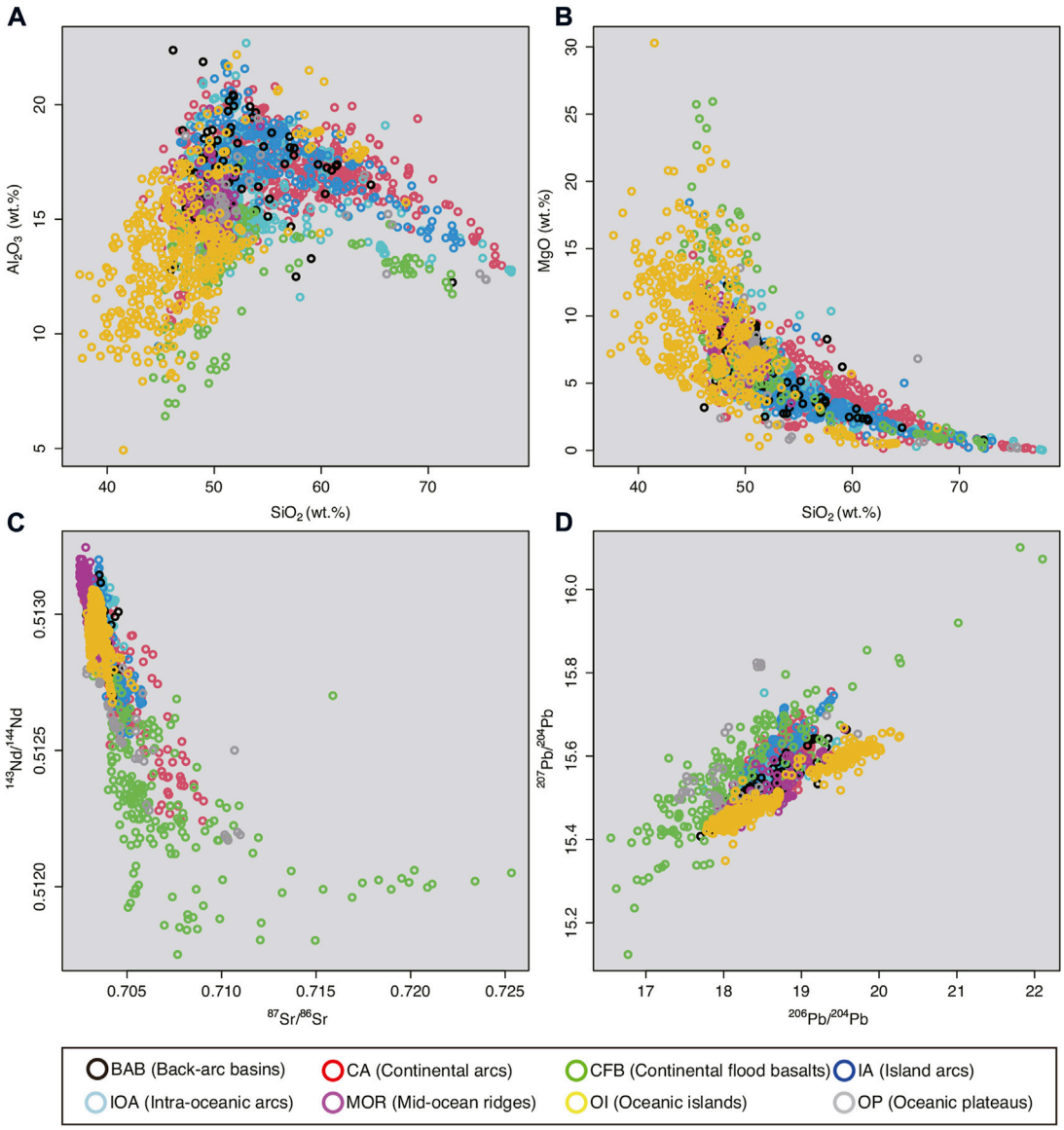

FIGURE 2
Variations in elemental concentrations and isotope ratios within the dataset used in this study. **(A)** SiO_2 *versus* Al_2O_3, **(B)** SiO_2 *versus* MgO, **(C)** $^{87}Sr/^{86}Sr$ *versus* $^{143}Nd/^{144}Nd$, and **(D)** $^{206}Pb/^{204}Pb$ *versus* $^{207}Pb/^{204}Pb$. The tectonic setting is indicated by the color of the symbols.

multinomial logistic regression (SMR) model. As such, the projection vector $\boldsymbol{w}$ is optimized by maximizing the ℓ_1 penalized log-likelihood function:

$$J(\boldsymbol{w},\lambda)=\sum_{i=1}^{n}\left\{\boldsymbol{w}^{(t(i))\top}\boldsymbol{x}_i-\log\left(\sum_{l=1}^{C}\exp\left(\boldsymbol{w}^{(l)\top}\boldsymbol{x}_i\right)\right)\right\}-n\lambda\|\boldsymbol{w}\|_1, \tag{4}$$

where λ is a hyperparameter, which defines the sparsity (i.e., sparsity-promoting parameter). With the sparse modeling approach, most elements of $\boldsymbol{w}$ are expected to be zero, meaning this approach enables the extraction of a small number of key features from a large number of variables.

Since λ was optimized to achieve high classification ability in our previous work (Ueki et al., 2018), selected variables were features relevant for classification rather than the representative characteristics of settings. Additionally, the selected variables included minor features that were used to characterize the entire compositional range (including end-members). As a result, although a sparse modeling approach was adopted in our previous study (Ueki et al., 2018), 17–28 variables were selected for each setting. To extract a

TABLE 1 SMR-based key geochemical variables for different tectonic settings. Variables are given in order of absolute values of w at a λ that corresponds to the first five variables while increasing λ.

Setting	Abbreviation	Selected key variables			
Mid-ocean ridges	MOR	Lu/Ba	Nb/Th	CaO×Yb	
Oceanic islands	OI	Nb/Rb	TiO_2/Lu		
Oceanic plateaus	OP	Gd/Sr	K_2O/Rb	Na_2O/Sr	
Continental flood basalts	CFB	Fe_2O_3/Al_2O_3	$^{87}Sr/^{86}Sr$		
Continental arcs	CA	Na_2O/Y	Ba/Y	Sr/Y	
Island arcs	IA	-La/Th	Yb/Gd	Th/Nb	
Intra-oceanic arcs	IOA	Fe_2O_3/Ta	K_2O/Nb	Ba/Th	SiO_2/Nb
Back arc basins	BAB	K_2O/Ba	CaO/Fe_2O_3		

small number of key features that are diagnostic of each tectono-magmatic setting, we started by varying λ. The solution paths generated by varying λ (Supplementary Figure S1) graphically describe the relationship between $\boldsymbol{w}$ and λ. With weaker sparseness (i.e., a small λ value), more variables are included in the model to describe the entire compositional range for classification purposes. With strong sparseness, only a small number of variables representing a majority of data points in a category are included in the model. Therefore, for feature extraction, we selected the variables included in the model under a large regularization parameter λ (Supplementary Table S2). We initially determined the first five variables that appeared whilst decreasing λ. Notably, two to four variables in each setting exhibit particularly high absolute values of w (Supplementary Table S2), meaning that these features can be regarded as key geochemical characteristics for these tectono-magmatic settings. Furthermore, to avoid biased results, we analyzed the first 5–10 variables that appeared for each setting, while increasing λ. The variables that were involved in all 5–10 cases were adopted as key features of each setting. This model-fitting procedure, involving varying the regularization parameter λ and selecting variables with high absolute w values in the first five variables, was applied to all eight tectono-magmatic settings. A small number of general and representative features for each setting were extracted. Key geochemical variables extracted from the 857 geochemical variables are given in Table 1. Changing the parameter λ affects the classification accuracy of the corresponding SMR model. However, in general, there is no monotonic dependence between the value of λ and classification accuracy of the model. In this study, a relatively high classification ability was achieved with strong sparseness (i.e., high λ value). Section 3.1 provides further details.

We used the R language (R Core Team, 2021) to implement the SMR. The R source code used during the analysis is provided on GitHub (https://github.com/hideitsu/geoSMR).

3 Results and discussion

3.1 Selected key geochemical features

Amongst the 22 geochemical features listed in Table 1, which include elemental ratios and multiplications, as well as isotope ratios, elemental ratios were the most frequently selected type of feature (i.e., selected 20 times). Well-documented trace element ratios such as Sr/Y (e.g., Defant and Drummond, 1990), Ta/Nb (Elliott et al., 1997), La/Th (e.g., Plank et al., 2007), Ba/Th (e.g., Pearce et al., 2005), Nb/Ba (e.g., Elliott et al., 1997), and K_2O/Rb (e.g., Hildreth and Moorbath, 1988) were also identified by our analysis. One isotope ratio ($^{87}Sr/^{86}Sr$) was selected. Although not commonly used in geochemical studies, one elemental multiplication (CaO×Yb) was also selected.

Using the representative λ value to obtain the results in Table 1 ($\lambda = 0.02$; see Supplementary Table S2), the classification accuracy of the SMR model based on the training data is 82.89 %. This relatively high classification accuracy means that the key variables listed in Table 1 can be used to identify the characteristics of unknown samples, and Figures 3, 4 can be used as geochemical discrimination diagrams. For example, Figure 3A clearly discriminates subduction zone-related settings from MOR and OI settings. It should be noted that BAB and OP have particularly low classification abilities with a high λ value (e.g., $\lambda = 0.02$), and thus high-dimensional data including multiple elements is necessary to obtain a high classification accuracy.

3.2 Global geochemical variations

Bivariate plots of the key geochemical features in Table 1 can be used to examine the geochemical similarities and differences between tectono-magmatic settings (Figures 3, 4). As an example, Figure 3A is described in detail here. Figure 3A shows a plot using two features selected for MOR settings (Lu/Ba and Nb/Th). In this plot, samples in the upper right exhibit a more MOR-like

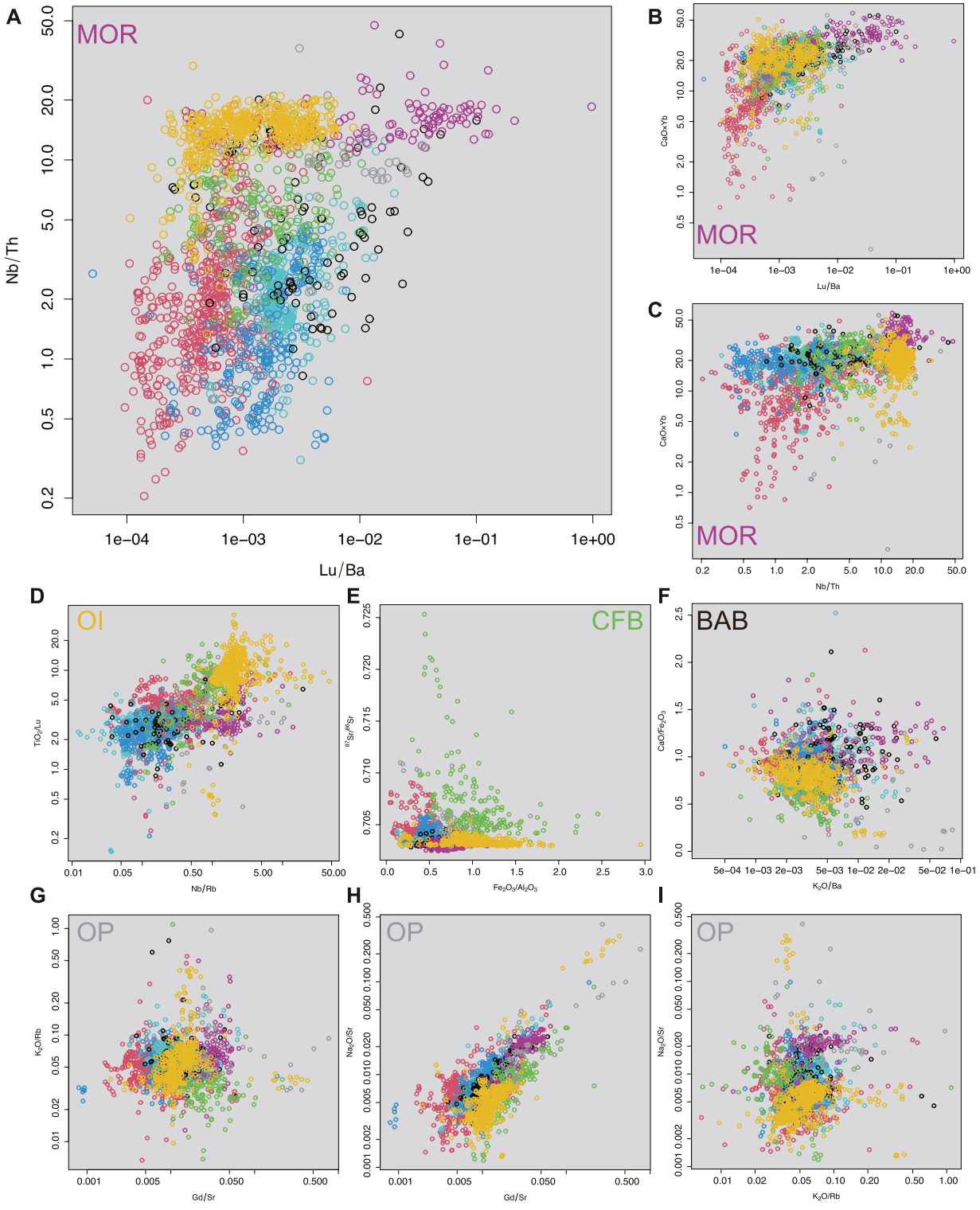

FIGURE 3
Bivariate plots of the key geochemical features (Table 1) of the MOR, OI, CFB, BAB, and OP settings. Symbols are as in Figure 2 **(A–C)** Geochemical features selected from MOR settings (Lu/Ba, Nb/Th, and CaO×Yb). Samples at upper right exhibit a more MOR-like signature. **(D)** Geochemical features selected from OI settings (Nb/Rb and TiO_2/Lu). Samples at upper right exhibit a more OI-like signature. **(E)** Geochemical features selected from CFB settings (Fe_2O_3/Al_2O_3 and $^{87}Sr/^{86}Sr$). Samples at upper right exhibit a more CFB-like signature. **(F)** Geochemical features selected from BAB settings (CaO/Fe_2O_3 and K_2O/Ba). Samples at upper right exhibit a more BAB-like signature. **(G–I)** Geochemical features selected from OP settings (Gd/Sr, K_2O/Rb, and Na_2O/Sr). Samples at upper right exhibit a more OP-like signature.

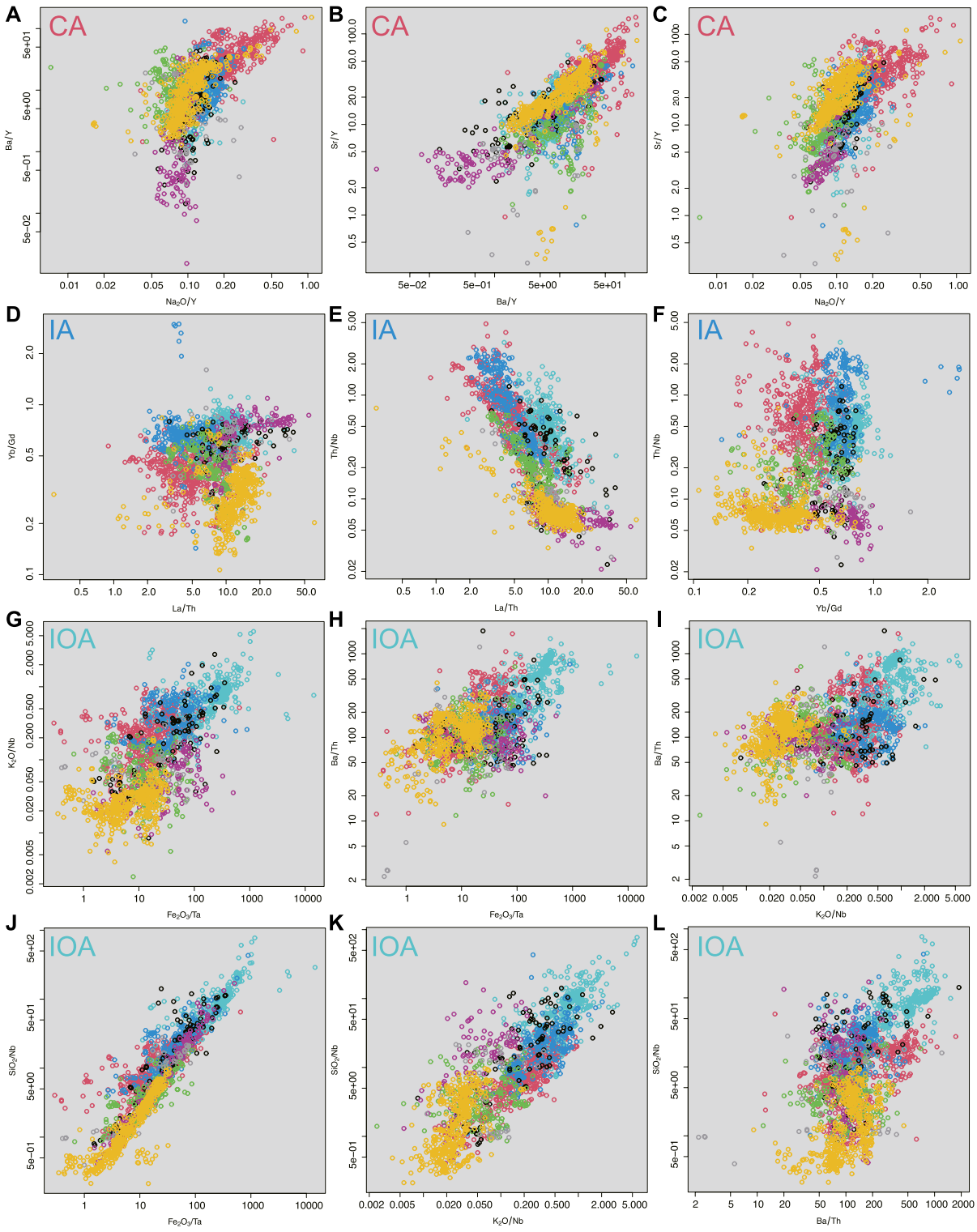

FIGURE 4
Bivariate plot of the key geochemical features (Table 1) of CA, IA, and IOA settings. Symbols are as in Figure 2. **(A–C)** Geochemical features selected from CA settings (Na_2O/Y, Ba/Y, and Sr/Y). Samples at upper right exhibit a more CA-like signature. **(D–F)** Geochemical features selected from IA settings (La/Th, Yb/Gd, and Th/Nb). On La/Th–Yb/Gd and La/Th–Th–Nb diagrams, samples at upper left exhibit a more IA-like signature. On a Yb/Gd–Th/Nb diagram, samples at upper right exhibit a more IA-like signature. **(G–L)** Geochemical features selected from IOA settings (Fe_2O_3/Ta, K_2O/Nb, Ba/Th, and SiO_2/Nb). Samples at upper right exhibit a more IOA-like signature.

signature, and samples in the lower-left exhibit a less MOR-like signature. In Figure 3A, MOR, OI, IOA, and CA settings represent end-members in the global magmatic dataset. MOR and OI have similar Nb/Th ratios, but different Lu/Ba ratios. All subduction-related settings (CA, IA, and IOA) have similar Nb/Th ratios, but different Lu/Ba ratios. Therefore, the *y*-axis (Nb/Th) in Figure 3A can be interpreted as a proxy for the involvement of subduction zone components, and the *x*-axis (Lu/Ba) can be interpreted as a proxy for contributions from enriched components such as fertile mantle, subduction-derived sediment components and crustal assimilation (i.e., the slope in a primitive-mantle normalized trace element diagram). OP magmas are mainly distributed between MOR and OI, whereas CFB magmas are mainly distributed between CA, IA, and OI. BAB magmas exhibit a wide compositional range and typically plot between MOR and IOA.

In the following section, we further discuss the details of the geochemical processes that operate in different tectono-magmatic settings.

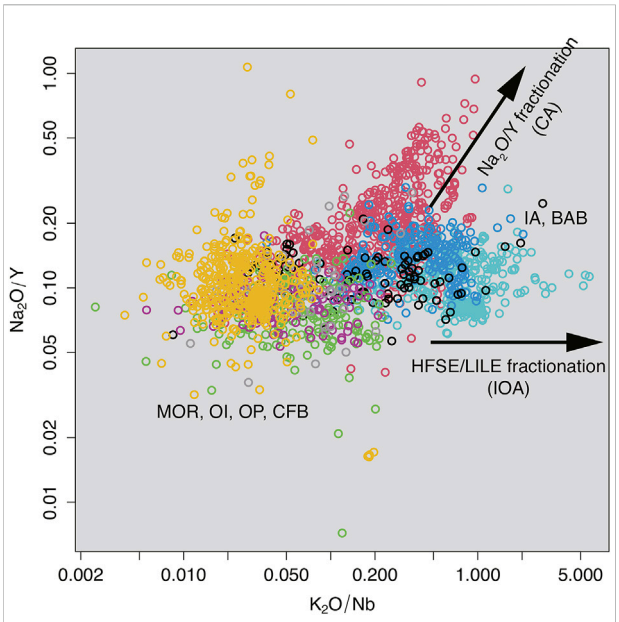

FIGURE 5
Bivariate plot of the key geochemical features for CA (Na_2O/Y) and IOA settings (K_2O/Nb). Symbols are as in Figure 2.

3.3 Geochemical processes in MOR, OI, OP, and CFB settings

Positive (i.e., relatively higher) Nb/Th, Lu/Ba, and CaO×Yb are identified as key features of MOR magmas. Based on Figure 3A, Nb/Th can be interpreted as a signature of a subduction-related component and Lu/Ba is indicative of fertility. Therefore, MOR magmas represent the depleted (Lu/Ba) end-member of global magmas with the least subduction-related component (Nb/Th). MOR magmas have elevated CaO×Yb compared with the other settings (Figure 3). Multiplication between element concentrations can be interpreted as a coupled enrichment, as MOR magmas have relatively high CaO and Yb concentrations (Ueki et al., 2018). Relatively elevated concentration of Yb in MOR settings have previously been interpreted as a signature of shallow melts with little or no garnet in the mantle source (Shen and Forsyth, 1995; Niu, 1997). The high CaO concentration can be interpreted to result from a depleted source, because melts generated by melting of a depleted mantle source typically have high CaO concentrations (Wasylenki et al., 2003). Consequently, the coupling of CaO and Yb indicates shallower melting of a depleted source in MOR settings. MOR magmas have a relatively narrow compositional range (Figures 3, 4), suggesting that homogeneous melts are generated in MOR settings by nominally anhydrous melting of the depleted mantle.

Selected features for OI magmas are elevated Nb/Rb and TiO_2/Lu values (Figure 3). These features are indicative of HFSE enrichment compared with LILEs and REEs, highlighting the subduction-related component-free (HFSE/LILE) and enriched (HFSE/REE) mantle melting processes involved in the formation of OI magmas.

Higher Gd/Sr, K_2O/Rb, and Na_2O/Sr are identified as features of OP magmas. High Gd/Sr (REE/LILE) and Na_2O/Sr reflect depletion of LILEs as compared with REEs and a major element, indicating subduction-related component are not involved in OP settings. K_2O/Rb may indicate a depleted source signature, because Rb is more incompatible than K (Pearce and Peate, 1995). Therefore, the key features for OP represent relatively depleted and anhydrous melting. In addition, OP magmas exhibit a MOR-like composition or an intermediate composition between MOR and OI magmas (Figure 3), indicating the melting of both OI-type fertile mantle and MOR-type depleted upper mantle. Indeed, paleogeographic studies based on seafloor magnetic anomalies have suggested that interaction between a mantle plume and a spreading ridge (i.e., melting of the shallow depleted mantle) is a critical factor in the generation of large-volume magmatism in OP settings (Sager et al., 2016).

Higher Fe/Al and $^{87}Sr/^{86}Sr$ ratios are identified as key features of CFB magmas. Figure 3E indicates that CFB and OI have the highest Fe/Al ratios of all the settings. High Fe/Al ratios have been previously identified as a key characteristic of CFB magmas (Pearce et al., 1977). Experimental studies have shown that the Fe concentrations of partial melts of the mantle increase with pressure, and Al concentrations decrease (e.g., Hirose and Kushiro, 1993; Walter, 1998). Consequently, a high Fe/Al ratio can be interpreted as reflecting relatively high-pressure melting during the generation of CFB magmas (Gibson et al., 2000). Fe_2O_3/Al_2O_3 ratios of >1 broadly correspond to melting

at pressures of >3 GPa (Walter, 1999). A pyroxenite-bearing source in the subcontinental lithospheric mantle could also explain the higher Fe/Al ratios (Swanson and Wright, 1981), because some pyroxenite melts have higher Fe and lower Al concentrations than melts from lherzolite (Borghini et al., 2017). CFB magmas have high $^{87}Sr/^{86}Sr$ ratios (Figure 3) that are comparable to those of CA magmas. High $^{87}Sr/^{86}Sr$ could be due to contributions from subcontinental lithospheric mantle that had been metasomatized by subduction-related components or extensive crustal contamination (Farmer, 2014). Indeed, involvement of metasomatized subcontinental lithospheric mantle is thought to be a significant factor in the generation of CFB magmas (e.g., White and McKenzie, 1995; Elkins Tanton and Hager, 2000; Elkins-Tanton, 2005). The fact that the CFB magmas are located between the OI and subduction-related settings in Figures 3, 4 also indicates a contribution from a subduction-related component in the generation of CFB magmas.

3.4 Geochemical processes in subduction-related settings

Figure 5 shows a bivariate plot of the selected features in CA (Na_2O/Y) and IOA (K_2O/Nb) settings, to emphasize the geochemical differences between subduction-related settings. Figure 5 shows that fractionation of Na_2O/Y is significant in CA magmas. In contrast, IOA magmas have a much narrower range of Na_2O/Y ratios, but a relatively large range of K_2O/Nb ratios. IA and BAB magmas are distributed between CA and IOA magmas. Other settings (MOR, OI, OP, and CFB) plot in the lower-left corner of the figure.

CA represent a hydrous (i.e., subduction fluid-fluxed) and fertile end-member of global magmas (Figures 3, 4), and Figure 5 highlights that fractionation of Na_2O/Y is particularly evident in CA settings. The Na_2O concentrations in subduction zone magmas exhibit a positive correlation with the thickness of underlying crust (e.g., Plank and Langmuir, 1988; Turner and Langmuir, 2015a,b; Turner et al., 2016), and higher Na_2O concentrations are inferred to represent low-degree melting in the mantle wedge beneath thicker arc crust (e.g., Plank and Langmuir, 1988; Turner et al., 2016). The depletion of Y is generally interpreted to be a signature of melts in equilibrium with a garnet-bearing residue (e.g., Defant and Drummond, 1990; Atherton and Petford, 1993; Van Westrenen et al., 1999). Prominent Na_2O/Y fractionation (Figures 4, 5) means that increasing Na_2O and decreasing Y are coupled in CA magmas, indicating relatively high-pressure melting of the mantle wedge beneath thick continental crust combined with garnet fractionation in the deep crust (Alonso-Perez et al., 2009) or partial melting of garnet-bearing lower crust (Annen et al., 2006). In addition, fractionation of Ba/Y and Sr/Y (LILE/REE) are selected features of CA magmas. In summary, the growth of REE-enriched and garnet-bearing lower crust, and LILE-enriched upper crust by intra-crustal magmatic processes, are both significant in CA settings (e.g., Lee et al., 2006).

Lower La/Th, higher Th/Nb, and higher Yb/Gd are key features of IA magmas. As discussed above for MOR magmas, the negative (i.e., relatively lower) La/Th ratios can be interpreted as a subduction signature. When compared with other subduction zone settings, IA magmas have an intermediate composition between CA and IOA in Figure 5. IA magmas have similar Th/Nb and La/Th ratios, but different Yb/Gd ratios, compared with CA magmas, and have similar Th/Nb and Yb/Gd ratios, but different La/Th ratios, as compared with IOA and BAB magmas (Figures 4D–F). Lower La/Th ratios have previously been interpreted as a signature of assimilation of evolved components such as sediments (Floyd and Leveridge, 1987; Plank et al., 2007) or crustal-derived silicic melts (Kimura and Yoshida, 2006). higher Yb/Gd (heavy REE/middle REE) values are indicative of a MORB-type flat or slightly middle to light-REE depleted chondrite-normalized REE pattern (i.e., depleted source), meaning that IA magmas represent subduction fluid-fluxed melting of depleted mantle, along with assimilation of a silicic (i.e., upper crustal) component.

Higher Fe_2O_3/Ta, K_2O/Nb, Ba/Th, and SiO_2/Nb ratios are key features of IOA magmas (Figure 4). High Ba/Th ratios indicate a contribution from an aqueous fluid component, because Ba is fluid mobile whereas Th is not, although both Th and Ba are incompatible elements (Pearce et al., 2005). IOA magmas exhibit a depleted signature in Figures 3, 4, suggesting minimum crustal assimilation. K_2O/Nb ratios record HFSE fractionation with respect to LILEs. Higher Fe_2O_3/Ta and SiO_2/Nb ratios indicate that the HFSEs are also depleted relative to major elements. In general, subduction zone magmas are characterized by depletion in HFSEs relative to REEs and LILEs (Pearce and Peate, 1995). We found that IOA settings show more prominent HFSE fractionation than other subduction zone settings (Figures 4, 5). This suggests that the geological setting of IOA, where one oceanic plate is being subducted beneath another, is particularly associated with significant depletion of HFSEs. IOA settings may involve a relatively shallow melting depth (Tamura et al., 2016) and a relatively warm mantle wedge due to the thinner overlying crust (Kincaid and Sacks, 1997). As such, a higher degree of fluid-fluxed melting (Kimura et al., 2009) or reactive transport of melt in the depleted oceanic lithosphere (Kelemen et al., 1990) could account for the enhanced depletion of HFSEs as compared with other subduction settings.

K_2O/Ba and CaO/Fe_2O_3 ratios are key features of BAB magmas. Higher K_2O/Ba ratios may indicate a depleted source signature, because both components are LILEs, and Ba is more incompatible than K (e.g., Pearce and Peate, 1995). As discussed above for MOR and CFB magmas, CaO/Fe_2O_3 is inferred to represent low-degree melting of a depleted source. In addition, BAB magmas exhibit a wide compositional range that overlaps those of OI, MOR, and IOA magmas, which suggests that various components are involved in the BAB magma source region (e.g., Ishizuka et al., 2009).

4 Summary

This study used a statistical model fitting method called sparse multinomial regression (SMR) to extract the key geochemical characteristics of magmas generated in different tectono-magmatic settings. A small number of key geochemical features, which can be interpreted in a geological and geochemical context, were identified based on our statistical approach. The methodology presented in this study is applicable to many geochemical fields of research.

We found that the magma generation processes in the mantle–crust system vary with the tectono-magmatic setting. MOR magmas are generated by anhydrous melting of depleted upper mantle and produce chemically homogeneous oceanic crust. OI magmas form by anhydrous melting of fertile mantle. OP magmas form by hybrid melting of fertile and MOR-type depleted mantle. CFB magmas are generated by high-pressure mantle melting and include contributions from metasomatized subcontinental lithospheric mantle and the continental crust. The key geochemical features of CA magmas indicate that net growth of the bulk continental crust occurs in a CA setting by growth of garnet-bearing lower crust and LILE-enriched upper crust. IA magmas are characterized by subduction fluid-fluxed melting of depleted mantle, and assimilation of silicic crustal material. IOA settings are characterized by simple subduction fluid-fluxed melting, with minimal crustal assimilation. Furthermore, our results indicate that depletion of HFSEs is enhanced in IOA settings relative to other subduction-related settings. BAB magmas are characterized by various mantle components, including MOR and OI type, as well as a subduction-related component. Subduction-related magmas (CA, IA, IOA, and BAB settings) each have distinct compositional ranges (Figures 3–5), meaning that chemical fractionation processes vary with the specific subduction setting. The geometry and thermal structure of the subducting slab and mantle wedge are important factors in controlling subduction zone magmatism (van Keken et al., 2011). Our analysis shows that differences in overriding plates (i.e., IOA, IA, and CA) are also important in generating different types of magmas (i.e., geochemical fractionations) in subduction zones. In addition, magmatism in each subduction-related setting has a relatively wide compositional range, indicating that the degree of geochemical fractionation involved in subduction zone processes varies even in one type of tectonic setting.

Data availability statement

The datasets presented in this study can be found in online repositories. The names of the repository/repositories and accession number(s) can be found in the article/Supplementary Material.

Author contributions

KU, HH and TK contributed to conception, methodology and design of the study. KU compiled the database and performed the age corrections for the isotope data. HH performed the statistical analysis. KU wrote the first draft of the manuscript. HH and TK wrote sections of the manuscript. All authors contributed to manuscript revision, read, and approved the submitted version.

Funding

This research was supported by JSPS KAKENHI Grants JP19K04026, JP20H01986, JP19K12111, JP19K04027, and JP22H03653, and JST CREST Grant JPMJCR1761.

Acknowledgments

We thank two reviewers for constructive reviews, and Nobuaki Fuji for editorial handling of the manuscript. Anonymous reviewers are thanked for useful and detailed comments on an earlier version of the manuscript. We thank the Cooperative Research Program of the Earthquake Research Institute, University of Tokyo (2018-B-01 and 2021-B-01), for discussion. We thank Takashi Miyazaki for discussions on the age corrections for the isotope data.

Conflict of interest

The authors declare that the research was conducted in the absence of any commercial or financial relationships that could be construed as a potential conflict of interest.

Publisher's note

Supplementary material

The Supplementary Material for this article can be found online at: https://www.frontiersin.org/articles/10.3389/feart.2022.994580/full#supplementary-material

References

Alonso-Perez, R., Müntener, O., and Ulmer, P. (2009). Igneous garnet and amphibole fractionation in the roots of island arcs: experimental constraints on andesitic liquids. *Contrib. Mineral. Pet.* 157, 541–558. doi:10.1007/s00410-008-0351-8

Annen, C., Blundy, J., and Sparks, R. (2006). The Genesis of intermediate and silicic magmas in deep crustal hot zones. *J. Petrology* 47, 505–539. doi:10.1093/petrology/egi084

Atherton, M. P., and Petford, N. (1993). Generation of sodium-rich magmas from newly underplated basaltic crust. *Nature* 362, 144–146. doi:10.1038/362144a0

Borghini, G., Fumagalli, P., and Rampone, E. (2017). Partial melting of secondary pyroxenite at 1 and 1.5 GPa, and its role in upwelling heterogeneous mantle. *Contrib. Mineral. Pet.* 172, 70. doi:10.1007/s00410-017-1387-4

Box, G. E. P., and Cox, D. R. (1964). An analysis of transformations. *J. R. Stat. Soc. Ser. B* 26, 211–243. doi:10.1111/j.2517-6161.1964.tb00553.x

Defant, M. J., and Drummond, M. S. (1990). Derivation of some modern arc magmas by melting of young subducted lithosphere. *Nature* 347, 662–665. doi:10.1038/347662a0

Elkins Tanton, L. T., and Hager, B. H. (2000). Melt intrusion as a trigger for lithospheric foundering and the eruption of the Siberian flood basalts. *Geophys. Res. Lett.* 27, 3937–3940. doi:10.1029/2000gl011751

Elkins-Tanton, L. T. (2005). Continental magmatism caused by lithospheric delamination. *Spec. Pap. Geol. Soc. Am.* 388, 449. doi:10.1130/0-8137-2388-4.449

Elliott, T., Plank, T., Zindler, A., White, W., and Bourdon, B. (1997). Element transport from slab to volcanic front at the Mariana arc. *J. Geophys. Res.* 102, 14991–15019. doi:10.1029/97jb00788

Farmer, G. (2014). "Continental basaltic rocks," in *Treatise geochem*. 2nd edn. (Netherland: Elsevier), 75–110.

Floyd, P., and Leveridge, B. (1987). Tectonic environment of the devonian gramscatho basin, south cornwall: framework mode and geochemical evidence from turbiditic sandstones. *J. Geol. Soc. Lond.* 144, 531–542. doi:10.1144/gsjgs.144.4.0531

Gibson, S., Thompson, R., and Dickin, A. (2000). Ferropicrites: geochemical evidence for Fe-rich streaks in upwelling mantle plumes. *Earth Planet. Sci. Lett.* 174, 355–374. doi:10.1016/s0012-821x(99)00274-5

Hildreth, W., and Moorbath, S. (1988). Crustal contributions to arc magmatism in the Andes of central Chile. *Contr. Mineral. Pet.* 98, 455–489. doi:10.1007/bf00372365

Hirose, K., and Kushiro, I. (1993). Partial melting of dry peridotites at high pressures: determination of compositions of melts segregated from peridotite using aggregates of diamond. *Earth Planet. Sci. Lett.* 114, 477–489. doi:10.1016/0012-821x(93)90077-m

Hofmann, A. (1997). Mantle geochemistry: the message from oceanic volcanism. *Nature* 385, 219–229. doi:10.1038/385219a0

Holden, N. E., Coplen, T. B., Böhlke, J. K., Tarbox, L. V., Benefield, J., de Laeter, J. R., et al. (2018). IUPAC periodic table of the elements and isotopes (IPTEI) for the education community (IUPAC technical report). *Pure Appl. Chem.* 90, 1833–2092. doi:10.1515/pac-2015-0703

Ishizuka, O., Yuasa, M., Taylor, R. N., and Sakamoto, I. (2009). Two contrasting magmatic types coexist after the cessation of back-arc spreading. *Chem. Geol.* 266, 274–296. doi:10.1016/j.chemgeo.2009.06.014

Itano, K., Ueki, K., Iizuka, T., and Kuwatani, T. (2020). Geochemical discrimination of monazite source rock based on machine learning techniques and multinomial logistic regression analysis. *Geosciences* 10, 63. doi:10.3390/geosciences10020063

Kelemen, P., Johnson, K., Kinzler, R., and Irving, A. (1990). High-field-strength element depletions in arc basalts due to mantle–magma interaction. *Nature* 345, 521–524. doi:10.1038/345521a0

Kimura, J.-I., Hacker, B. R., van Keken, P. E., Kawabata, H., Yoshida, T., and Stern, R. J. (2009). Arc Basalt Simulator version 2, a simulation for slab dehydration and fluid-fluxed mantle melting for arc basalts: Modeling scheme and application. *Geochem. Geophys. Geosyst.* 10, Q09004. doi:10.1029/2008gc002217

Kimura, J.-I., and Yoshida, T. (2006). Contributions of slab fluid, mantle wedge and crust to the origin of Quaternary lavas in the NE Japan arc. *J. Petrology* 47, 2185–2232. doi:10.1093/petrology/egl041

Kincaid, C., and Sacks, I. S. (1997). Thermal and dynamical evolution of the upper mantle in subduction zones. *J. Geophys. Res.* 102, 12295–12315. doi:10.1029/96jb03553

Lee, C.-T. A., Cheng, X., and Horodyskyj, U. (2006). The development and refinement of continental arcs by primary basaltic magmatism, garnet pyroxenite accumulation, basaltic recharge and delamination: insights from the sierra Nevada, California. *Contrib. Mineral. Pet.* 151, 222–242. doi:10.1007/s00410-005-0056-1

Li, C., Arndt, N. T., Tang, Q., and Ripley, E. M. (2015). Trace element indiscrimination diagrams. *Lithos* 232, 76–83. doi:10.1016/j.lithos.2015.06.022

National Geophysical Data Center/NESDIS/NOAA/U.S. Department of Commerce (1995). *Terrainbase, global 5 arc-minute ocean depth and land elevation from the US national geophysical data center (NGDC)*. USA: US national geophysical data center.

Nelder, J. A., and Wedderburn, R. W. (1972). Generalized linear models. *J. R. Stat. Soc. Ser. A* 135, 370–384. doi:10.2307/2344614

Niu, Y. (1997). Mantle melting and melt extraction processes beneath ocean ridges: evidence from abyssal peridotites. *J. Petrology* 38, 1047–1074. doi:10.1093/petroj/38.8.1047

Pearce, J. A., and Peate, D. W. (1995). Tectonic implications of the composition of volcanic arc magmas. *Annu. Rev. Earth Planet. Sci.* 23, 251–285. doi:10.1146/annurev.ea.23.050195.001343

Pearce, J. A., Stern, R. J., Bloomer, S. H., and Fryer, P. (2005). Geochemical mapping of the Mariana arc–basin system: Implications for the nature and distribution of subduction components. *Geochem. Geophys. Geosyst.* 6, Q07006. doi:10.1029/2004gc000895

Pearce, T. H., Gorman, B., and Birkett, T. (1977). The relationship between major element chemistry and tectonic environment of basic and intermediate volcanic rocks. *Earth Planet. Sci. Lett.* 36, 121–132. doi:10.1016/0012-821x(77)90193-5

Petrelli, M., and Perugini, D. (2016). Solving petrological problems through machine learning: the study case of tectonic discrimination using geochemical and isotopic data. *Contrib. Mineral. Pet.* 171, 81. doi:10.1007/s00410-016-1292-2

Plank, T., Kelley, K. A., Murray, R. W., and Stern, L. Q. (2007). Chemical composition of sediments subducting at the Izu–Bonin trench. *Geochem. Geophys. Geosyst.* 8, Q04I16. doi:10.1029/2006gc001444

Plank, T., and Langmuir, C. H. (1988). An evaluation of the global variations in the major element chemistry of arc basalts. *Earth Planet. Sci. Lett.* 90, 349–370. doi:10.1016/0012-821x(88)90135-5

R Core Team (2021). *R: A language and environment for statistical computing*. Vienna, Austria: R Foundation for Statistical Computing.

Sager, W. W., Sano, T., and Geldmacher, J. (2016). Formation and evolution of Shatsky Rise oceanic plateau: Insights from IODP Expedition 324 and recent geophysical cruises. *Earth. Sci. Rev.* 159, 306–336. doi:10.1016/j.earscirev.2016.05.011

Shen, Y., and Forsyth, D. W. (1995). Geochemical constraints on initial and final depths of melting beneath mid-ocean ridges. *J. Geophys. Res.* 100, 2211–2237. doi:10.1029/94jb02768

Stracke, A. (2012). Earth's heterogeneous mantle: A product of convection-driven interaction between crust and mantle. *Chem. Geol.* 330, 274–299. doi:10.1016/j.chemgeo.2012.08.007

Swanson, D. A., and Wright, T. L. (1981). *The regional approach to studying the columbia river basalt group*, 3. India: Geological Society of India.

Tamura, Y., Sato, T., Fujiwara, T., Kodaira, S., and Nichols, A. (2016). Advent of continents: A new hypothesis. *Sci. Rep.* 6, 33517. doi:10.1038/srep33517

Tibshirani, R. (1996). Regression shrinkage and selection via the lasso. *J. R. Stat. Soc. Ser. B* 58, 267–288. doi:10.1111/j.2517-6161.1996.tb02080.x

Turner, S. J., Langmuir, C. H., Katz, R. F., Dungan, M. A., and Escrig, S. (2016). Parental arc magma compositions dominantly controlled by mantle-wedge thermal structure. *Nat. Geosci.* 9, 772–776. doi:10.1038/ngeo2788

Turner, S. J., and Langmuir, C. H. (2015a). The global chemical systematics of arc front stratovolcanoes: Evaluating the role of crustal processes. *Earth Planet. Sci. Lett.* 422, 182–193. doi:10.1016/j.epsl.2015.03.056

Turner, S. J., and Langmuir, C. H. (2015b). What processes control the chemical compositions of arc front stratovolcanoes? *Geochem. Geophys. Geosyst.* 16, 1865–1893. doi:10.1002/2014gc005633

Ueki, K., Hino, H., and Kuwatani, T. (2018). Geochemical discrimination and characteristics of magmatic tectonic settings: A machine-learning-based approach. *Geochem. Geophys. Geosyst.* 19, 1327–1347. doi:10.1029/2017gc007401

van Keken, P. E., Hacker, B. R., Syracuse, E. M., and Abers, G. A. (2011). Subduction factory: 4. depth-dependent flux of H_2O from subducting slabs worldwide. *J. Geophys. Res.* 116, B01401. doi:10.1029/2010jb007922

Van Westrenen, W., Blundy, J., and Wood, B. (1999). Crystal-chemical controls on trace element partitioning between garnet and anhydrous silicate melt. *Am. Mineral.* 84, 838–847. doi:10.2138/am-1999-5-617

Walter, M. J. (1998). Melting of garnet peridotite and the origin of komatiite and depleted lithosphere. *J. Petrology* 39, 29–60. doi:10.1093/petroj/39.1.29

Walter, M. J. (1999). Melting residues of fertile peridotite and the origin of cratonic lithosphere. *Spec. Publ. Geochem. Soc.* 6, 225–239.

Wasylenki, L. E., Baker, M. B., Kent, A. J., and Stolper, E. M. (2003). Near-solidus melting of the shallow upper mantle: partial melting experiments on depleted peridotite. *J. Petrology* 44, 1163–1191. doi:10.1093/petrology/44.7.1163

White, R., and McKenzie, D. (1995). Mantle plumes and flood basalts. *J. Geophys. Res.* 100, 17543–17585. doi:10.1029/95jb01585

Wilson, B. M. (2007). *Igneous petrogenesis: a global tectonic approach*. Berlin: Springer Science & Business Media.

Wyllie, P. J. (1988). Magma Genesis, plate tectonics, and chemical differentiation of the Earth. *Rev. Geophys.* 26, 370–404. doi:10.1029/rg026i003p00370

Zhao, Y., Zhang, Y., Geng, M., Jiang, J., and Zou, X. (2019). Involvement of slab-derived fluid in the generation of Cenozoic basalts in Northeast China inferred from machine learning. *Geophys. Res. Lett.* 46, 5234–5242. doi:10.1029/2019gl082322